Journal of Zhejiang University-SCIENCE C (Computers & Electronics)
ISSN 1869-1951 (Print); ISSN 1869-196X (Online)
www.zju.edu.cn/jzus; www.springerlink.com
E-mail: jzus@zju.edu.cn

A modified direct adaptive robust motion trajectory tracking controller of a pneumatic system

Peng-fei QIAN[†1], Guo-liang TAO[1], De-yuan MENG[2], Hao LIU[1]

([1]*The State Key Laboratory of Fluid Power Transmission and Control, Zhejiang University, Hangzhou 310027, China*)

([2]*School of Mechatronic Engineering, China University of Mining and Technology, Xuzhou 221116, China*)

[†]E-mail: pengfeiqian@zju.edu.cn

Received Jan. 5, 2014; Revision accepted Apr. 16, 2014; Crosschecked Sept. 17, 2014

Abstract: In this study, we developed and tested a high-precision motion trajectory tracking controller of a pneumatic cylinder driven by four costless on/off solenoid valves rather than by a proportional directional control valve. The relationship between the pulse width modulation (PWM) of a signal's duty cycle and control law was determined experimentally, and a mathematical model of the whole system established. Owing to unknown disturbances and unmodeled dynamics, there are considerable uncertain nonlinearities and parametric uncertainties in this pneumatic system. A modified direct adaptive robust controller (DARC) was constructed to cope with these issues. The controller employs a gradient type adaptation law based on discontinuous projection mapping to guarantee that estimated unknown model parameters stay within a known bounded region, and uses a deterministic robust control strategy to weaken the effects of unmodeled dynamics, disturbances, and parameter estimation errors. By using discontinuous projection mapping, the parameter adaptation law and the robust control law can be synthesized separately. A recursive backstepping technology is applied to account for unmatched model uncertainties. Kalman filters were designed separately to estimate the motion states and the derivative of the intermediate control law in synthesizing the deterministic robust control law. Experimental results illustrate the effectiveness of the proposed controller.

Key words: On/off solenoid valve, Tracking control, Robust control, Adaptive control, Kalman filter, Discontinuous projection
doi:10.1631/jzus.C1400003 **Document code:** A **CLC number:** TH138; TP273

1 Introduction

Pneumatic actuators are common in industrial applications because of their high power-to-mass ratio, low cost, clean operation, and easy maintenance (Aziz and Bone, 1998). Although highly nonlinear dynamics and many model uncertainties are caused by gas compressibility, flow characteristics, and friction characteristics in a pneumatic system, the realization of a high-accuracy trajectory tracking is possible through technical improvement.

In the field of servo control of pneumatic cylinders, conventional linear controllers (Brun *et al.*, 1999) and modified conventional linear controllers (Richard and Scavarda, 1996; van Varseveld and Bone, 1997; Wang *et al.*, 2001; Lee *et al.*, 2002; Schulte and Hahn, 2004; Situm *et al.*, 2004; Xiang and Wikander, 2004; Ahn and Yokota, 2005) have mostly been used. In recent years, nonlinear controls, such as adaptive control (Richardson *et al.*, 2001), sliding mode control (Ning and Bone, 2005; Chen *et al.*, 2009; Girin *et al.*, 2009), and backstepping control (Smaoui *et al.*, 2006; Rao and Bone, 2008; Tsai and Huang, 2008; Carneiro and de Almeida, 2012), have been extensively applied to address this issue. In general, to achieve better performance from servo control of pneumatic cylinders, nonlinear control strategies are the preferred choice.

Theoretically, the tracking error can be reduced infinitely through direct strong feedback action. However, asymptotical tracking cannot be achieved unless the control law is allowed to be discontinuous

or some equivalent gains in the control law approach infinity. Neither way is practical since they will inevitably excite neglected high frequency unmodeled dynamics (Yao and Tomizuka, 1997). In contrast, adaptive control uses indirect feedback means, such as online parameter adaptation, to reduce modeling uncertainties. Therefore, to achieve better performance, the original direct adaptive robust control (DARC) (Yao and Tomizuka, 1997), a promising control strategy integrating the advantages of deterministic robust control (DRC) and adaptive control (AC), needs to be employed. Experimental tests have proved that DARC is quite effective for systems with uncertain nonlinearities and parametric uncertainties (Yao *et al.*, 2000; Xu and Yao, 2001; Zhu *et al.*, 2008; Meng *et al.*, 2013a). Nevertheless, during the synthesis of the robust control law applying the recursive backstepping technology, the solution to the calculable part of the derivative of the intermediate control law requires a large amount of computation time. Moreover, the more parameters that are estimated, the more computation time may be consumed. Among the studies cited above, one or more expensive proportional valves are used in the valve-controlled pneumatic cylinder systems for achieving high-accuracy trajectory tracking. However, some studies of nonlinear servo control of valve-controlled pneumatic cylinder systems have considered the use of costless on/off solenoid valves. For example, Barth *et al.* (2002) provided a method to transform the non-analytic description of the pulse width modulation (PWM) based control of a pneumatic system into an analytic model. The combination of sliding mode control and PWM was then tested. Tracking results were demonstrated for a sinusoidal trajectory motion with an amplitude of 25 mm and a payload of 10 kg at various frequencies from 0.1 to 1.25 Hz. Barth and Goldfarb (2002) formulated a control design method for a pneumatic system with a finite number of discrete input values. The proposed control design method was applied to a pneumatic positioning system consisting of a time-delayed linear time invariant (LTI) switching system. A sinusoidal trajectory with an amplitude of 25 mm at different frequencies (0.5, 1, 2, and 3 Hz) was tracked to test the tracking performance. Shen *et al.* (2006) developed an averaging approach to describe the equivalent continuous-time dynamics of a PWM controlled nonlinear system. A sliding mode controller was developed based on the averaged equivalent control canonical form. The peak tracking errors at various frequencies for a sinusoidal trajectory with a 20-mm amplitude and a 10-kg payload were all over 10% of the desired signal amplitude. Hodgson *et al.* (2012) introduced a novel seven-mode sliding mode controller for a pneumatic actuator with four on/off solenoid valves. The proposed control was successfully implemented in simulations and experiments. However, there were no data on robustness in these studies. Nguyen *et al.* (2007) developed an inexpensive pneumatic motion control system using only four on/off solenoid valves and a displacement sensor. A sliding mode control law with a dead-zone design was implemented, but not in the form of PWM. A low-amplitude 20-mm sinusoidal trajectory tracking motion at 0.5 Hz was executed with an approximate 2-mm peak error. The robustness was demonstrated by varying the payload for the experiment from 50% to 400% of its nominal value. However, although a model's uncertainty effects can be overpowered through strong nonlinear robust feedback, the above nonlinear controllers will suffer from severe control input chattering. Furthermore, since these pneumatic systems have large variations in their parameters, high-accuracy tracking is difficult to achieve because of a lack of online parameter adaptation.

In this paper, a pneumatic cylinder controlled by four costless on/off solenoid valves is considered, and a modified DARC is proposed to achieve high-precision motion trajectory tracking control for the pneumatic system.

2 Dynamic models

Fig. 1 shows a schematic diagram of the pneumatic system under consideration, which consists of a pneumatic cylinder controlled by four on/off solenoid valves. The solenoid valves, adopting PWM technology, regulate the effective orifice areas through the PWM duty cycles. To simplify the analysis, some assumptions (Qian *et al.*, 2012) need to be made. The pressure in the chamber is assumed to be uniform, because the pressure spreads with the velocity of sound. It is assumed that the gas is perfect, which satisfies the ideal gas law and the law of conservation

of mass, and that there is no leakage in the chamber or the connecting tube. The effects of time delay and attenuation caused by the connecting tubes between the valve and cylinder are also neglected.

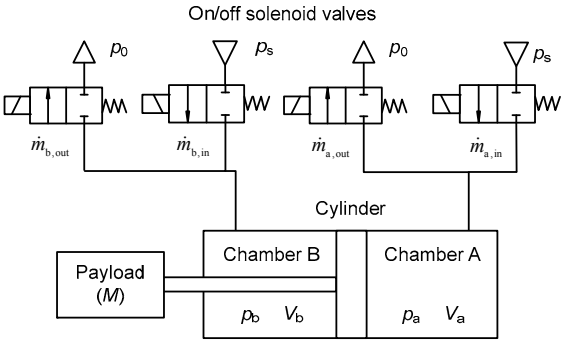

Fig. 1 Schematic diagram of a pneumatic cylinder controlled by four on/off solenoid valves

2.1 Models of a pneumatic cylinder

According to Newton's second law of motion, the motion of the piston, as a result of the external disturbance force, friction, and pressure forces, is as follows:

$$M\ddot{x} = p_a A_a - p_b A_b - p_0 A_r - F_f + \tilde{F}, \tag{1}$$

where x is the piston position, p_a, p_b, p_0 are the absolute pressures, subscripts 'a', 'b', and '0' refer to chamber A, chamber B, and ambience, respectively, M is the effective mass of the moving parts, A_a, A_b, and A_r are the effective piston areas and the cross-sectional area of the piston rod, respectively, F_f is the friction force, and $\tilde{F}$ is the lumped modeling error, including external disturbances and terms like the unmodeled friction forces and uncertainties.

The friction force may be modeled as a combination of viscous friction, Coulomb friction, and the component due to the Stribeck effect. A simplified model of pneumatic cylinder friction force can be described by

$$F_f = \begin{cases} \left[F_C + (F_S - F_C)\exp\left(-\left|\dot{x}/\dot{x}_S\right|^{\alpha}\right)\right]\operatorname{sgn}(\dot{x}) + b_v\dot{x}, \\ \qquad \text{if } \dot{x} \neq 0, \\ F_e, \qquad \text{otherwise}, \end{cases} \tag{2}$$

where F_S is the stiction force, F_C is the dynamic Coulomb friction level, b_v is the viscous friction coefficient, $\dot{x}_S$ is the Stribeck velocity, α is the exponent for the Stribeck curve, and F_e is the external force acting on the piston. All these parameters can be estimated or measured by experiments, as described by Qian *et al.* (2012). Since the friction model is discontinuous at zero velocity, it may excite the neglected high-frequency dynamics when such a model is used for friction compensation. So, we need a smooth approximation model which has the same characteristics as the friction force model (2) when the velocity is not in a low region, to represent model (2):

$$\hat{F}_f = b_v\dot{x} + A_f S_f(\dot{x}), \tag{3}$$

where A_f is the amplitude of the Coulomb friction force and $S_f(\dot{x})$ is a known smooth function, which can be chosen as

$$S_f(\dot{x}) = \frac{2}{\pi}\arctan(1000\dot{x}). \tag{4}$$

To simplify the design of the controller, the process of heat transfer between the gas and the cylinder wall is not modeled directly but is contained in the lumped modeling error. Furthermore, to facilitate the controller's simplified design, the gas temperature inside the chamber is assumed to be constant and equal to the ambient temperature. According to the conservation-of-mass equation, the first law of thermodynamics, and the ideal gas law, the differential equations that describe the thermodynamic process of gas in a pneumatic cylinder can be expressed as

$$\begin{cases} \dot{p}_i = -\dfrac{np_i\dot{V}_i}{V_i} + \dfrac{nRT_i\dot{m}_i}{V_i} + \tilde{D}_i, \\ T_i = T_0, \end{cases} \tag{5}$$

where i=a or b, n is the polytropic exponent ranging from 1.0 for an isothermal process to 1.4 for an adiabatic process, R is the universal gas constant, T and p are the gas temperature and absolute pressure, respectively, inside the chamber, $\dot{m}$ represents the net mass flow rate, which is positive while charging the chamber and negative while discharging to the atmosphere, T_0 is the ambient temperature, $\tilde{D}$ is the lumped modeling error, including external disturbances and terms like the neglected temperature

dynamics and uncertainties, V is the volume of the chamber, and subscripts 'a' and 'b' represent properties of chambers A and B, respectively. Choosing the origin of the displacement sensor at a position approximately 1.5 mm away from the end of the rodless chamber, the volume of the chambers can be expressed as

$$\begin{cases} V_{\mathrm{a}} = V_{0\mathrm{a}} + A_{\mathrm{a}}(0.0015 + x), \\ V_{\mathrm{b}} = V_{0\mathrm{b}} + A_{\mathrm{b}}(0.0485 - x), \end{cases} \tag{6}$$

where $V_{0\mathrm{a}}$ and $V_{0\mathrm{b}}$ represent the dead volumes of the rodless chamber and rod chamber, respectively, at the end of the stroke, including lines and fittings.

2.2 Flow-rate model of an on/off solenoid valve

Due to the use of the on/off solenoid valve with PWM, the flow rate is discontinuous for valves constantly switching between fully open and fully closed. The pressure dynamics of Eq. (5) are governed in part by the mass flow-rate term which, in turn, is influenced by the commanded duty ratio of PWM. The flow-rate characteristic of an on/off solenoid valve is represented by the standard ISO 6358, based on the model of a converging nozzle. The governing equation of the mass flow through the on/off valve port can be expressed as

$$\dot{m} = \begin{cases} C\rho_0 p_{\mathrm{u}} \sqrt{T_0 / T_{\mathrm{u}}}, & \dfrac{p_{\mathrm{d}}}{p_{\mathrm{u}}} \le b, \\ C\rho_0 p_{\mathrm{u}} \sqrt{\dfrac{T_0}{T_{\mathrm{u}}}} \sqrt{1 - \left(\dfrac{p_{\mathrm{d}}/p_{\mathrm{u}} - b}{1 - b} \right)^2}, & b < \dfrac{p_{\mathrm{d}}}{p_{\mathrm{u}}} \le 1, \end{cases} \tag{7}$$

where C is the sonic conductance, ρ_0 is the density of air under standard conditions, b is the critical pressure ratio, p_{u} and T_{u} are the upstream absolute pressure and temperature, respectively, and p_{d} is the downstream absolute pressure.

2.3 System dynamics

Generally, the system is subject to parametric uncertainties owing to the variation of b_{v}, A_{f}, F_{l} and uncertain nonlinearities represented by $\tilde{F}$, $\tilde{D}_{\mathrm{a}}$, and $\tilde{D}_{\mathrm{b}}$ that arise from some model terms due to unknown model errors and disturbances. Here, uncertain nonlinearities may be theoretically segmented into two components, a fast changing part denoted by $\tilde{F}_0$, $\tilde{D}_{\mathrm{a}0}$, and $\tilde{D}_{\mathrm{b}0}$, and a constant part denoted by F_{n}, D_{an}, and D_{bn}. To employ parameter adaptation to reduce parametric uncertainties for an improved performance, the system's dynamic models can be linearly parametrized in terms of a set of unknown parameters. Here, we define the unknown parameter set $\boldsymbol{\theta}=[\theta_1, \theta_2, \theta_3, \theta_4, \theta_5, \theta_6]^{\mathrm{T}}$ as $\theta_1=M$, $\theta_2=F_{\mathrm{n}}$, $\theta_3=b_{\mathrm{v}}$, $\theta_4=A_{\mathrm{f}}$, $\theta_5=D_{\mathrm{an}}$, and $\theta_6=D_{\mathrm{bn}}$, and define a set of state variables as $\boldsymbol{x}=[x_1, x_2, x_3, x_4]^{\mathrm{T}}=[x, \dot{x}, p_{\mathrm{a}}, p_{\mathrm{b}}]^{\mathrm{T}}$. For simplicity, the following notations are used throughout the paper: $\bullet_i$ is used for the ith component of the vector $\bullet$, the operation '$\le$' for two vectors is performed in terms of the corresponding elements of the vectors, and the notations $\hat{\bullet}$ and $\tilde{\bullet}$ represent the estimate and the estimation error, respectively, of $\bullet$. The whole system dynamics can be simply expressed in a state-space form as

$$\begin{cases} \dot{x}_1 = x_2, \\ \theta_1 \dot{x}_2 = (A_{\mathrm{a}} x_3 - A_{\mathrm{b}} x_4 - p_0 A_{\mathrm{r}}) + \theta_2 - \theta_3 x_2 \\ \qquad\quad -\theta_4 S_{\mathrm{f}}(x_2) + \tilde{F}_0, \\ \dot{x}_3 = \dfrac{nR}{V_{\mathrm{a}}}(\dot{m}_{\mathrm{a,in}} T_0 - \dot{m}_{\mathrm{a,out}} T_{\mathrm{a}}) - \dfrac{nA_{\mathrm{a}} x_2 x_3}{V_{\mathrm{a}}} + \theta_5 + \tilde{D}_{\mathrm{a}0}, \\ \dot{x}_4 = \dfrac{nR}{V_{\mathrm{b}}}(\dot{m}_{\mathrm{b,in}} T_0 - \dot{m}_{\mathrm{b,out}} T_{\mathrm{b}}) + \dfrac{nA_{\mathrm{b}} x_2 x_4}{V_{\mathrm{b}}} + \theta_6 + \tilde{D}_{\mathrm{b}0}, \end{cases} \tag{8}$$

where $\dot{m}_{\mathrm{a,in}}$ and $\dot{m}_{\mathrm{a,out}}$ denote the mass flows entering and leaving the non-rod chamber, respectively. Similarly, for $\dot{m}_{\mathrm{b,in}}$ and $\dot{m}_{\mathrm{b,out}}$, as the parametric uncertainties and modeling errors are both bounded and can be predicted roughly, the following practical assumption is made:

Assumption 1 The extent of parametric uncertainties and uncertain nonlinearities is known, i.e., $\boldsymbol{\theta} \in \Omega_{\boldsymbol{\theta}} = \{\boldsymbol{\theta}: \ \boldsymbol{\theta}_{\min} \le \boldsymbol{\theta} \le \boldsymbol{\theta}_{\max}\}$, $\left|\tilde{F}_0(t)\right| \le F_{\max}$, $\left|\tilde{D}_{\mathrm{a}0}(t)\right| \le D_{\mathrm{a}\max}$, $\left|\tilde{D}_{\mathrm{b}0}(t)\right| \le D_{\mathrm{b}\max}$, where $\boldsymbol{\theta}_{\min}=[\theta_{1\min}, \theta_{2\min}, \ldots, \theta_{6\min}]^{\mathrm{T}}$ is the minimum parameter vector, $\boldsymbol{\theta}_{\max}=[\theta_{1\max}, \theta_{2\max}, \ldots, \theta_{6\max}]^{\mathrm{T}}$ is the maximum parameter vector, and $F_{\max}$, $D_{\mathrm{a}\max}$, and $D_{\mathrm{b}\max}$ are known scalars.

3 Controller design

The main objective of this section is to synthesize a control input u by applying a modified DARC

to the system, so that x_1 tracks the desired trajectory $x_{1\mathrm{r}}$ with a guaranteed transient and steady-state tracking. First, a rate-limited projection type should be used to perform the adaptation process, as described below.

3.1 Rate-limited projection type adaptation law

To separate completely robust control law design and parameter estimator design, in addition to the use of the projection type parameter adaptation law, it is necessary to preset a limit on the adaptation rate for a controlled estimation process (Yao, 2003). Hence, the parameter estimate $\hat{\boldsymbol{\theta}}$ can be updated using the following rate-limited projection type adaptation law with a preset adaptation rate limit $\dot{\boldsymbol{\theta}}_M$:

$$\dot{\hat{\boldsymbol{\theta}}} = \mathrm{sat}_{\dot{\theta}_M}\left(\mathbf{Proj}_{\hat{\theta}}(\boldsymbol{\Gamma\tau})\right), \tag{9}$$

where $\mathrm{sat}_{\dot{\theta}_M}(\bullet)$ is a saturation function, $\boldsymbol{\tau}$ is the estimation function, $\boldsymbol{\Gamma}$ is a positive definite diagonal adaptation rate matrix, and $\mathbf{Proj}_{\hat{\theta}}(\boldsymbol{\Gamma\tau})$ is a simple discontinuous projection mapping defined by $\mathbf{Proj}_{\hat{\theta}}(\bullet)=[\mathrm{Proj}_{\hat{\theta}_1}(\bullet_1),\cdots,\mathrm{Proj}_{\hat{\theta}_6}(\bullet_6)]^{\mathrm{T}}$, where

$$\mathrm{Proj}_{\hat{\theta}_i}(\bullet_i)=\begin{cases}0, & \text{if } \hat{\theta}_i=\hat{\theta}_{i\max} \text{ and } \bullet_i>0,\\ & \text{or } \hat{\theta}_i=\hat{\theta}_{i\min} \text{ and } \bullet_i<0,\\ \bullet_i, & \text{otherwise,}\end{cases} \tag{10}$$

i=1, 2, …, 6.

The saturation function mentioned in Eq. (9) is defined as

$$\mathrm{sat}_{\dot{\theta}_M}(\bullet)_i=\begin{cases}\bullet_i, & |\bullet_i|\le\dot{\theta}_{Mi},\\ \dot{\theta}_{Mi}\,\mathrm{sgn}(\bullet_i), & |\bullet_i|>\dot{\theta}_{Mi},\end{cases} \quad i=1, 2, \ldots, 6. \tag{11}$$

where $\dot{\boldsymbol{\theta}}_M$ is the preset adaptation rate limit.

Yao and Tomizuka (1994; 1997) showed that with the above-mentioned adaptation law structure, the parameter estimates always stay within a known bounded region and the parameter adaptation rate is uniformly bounded for any estimation function. According to Yao and Palmer (2002), all the guaranteed properties can be expressed as follows:

$$\begin{cases}\hat{\boldsymbol{\theta}}(t)\in\Omega_\theta=\left\{\hat{\boldsymbol{\theta}}:\boldsymbol{\theta}_{\min}\le\hat{\boldsymbol{\theta}}\le\boldsymbol{\theta}_{\max}\right\} \ \ \forall t,\\ \tilde{\boldsymbol{\theta}}^{\mathrm{T}}\left[\boldsymbol{\Gamma}^{-1}\mathbf{Proj}_{\hat{\theta}}(\boldsymbol{\Gamma\tau})-\boldsymbol{\tau}\right]\le 0 \ \ \forall\boldsymbol{\tau},\\ \left|\dot{\hat{\theta}}(t)_i\right|\le\dot{\theta}_{Mi},\ i=1,2,\cdots,6 \ \ \forall t.\end{cases} \tag{12}$$

Thus, estimator design and robust control law design can be separated completely.

3.2 Modified DARC controller design

To facilitate the design of the control law, a switching schema consisting of three operation modes for the solenoid valve-controlled pneumatic cylinder system (Fig. 1) is defined as follows:

Mode 1: u>0 denotes that chamber A fills and chamber B exhausts.

Mode 2: u<0 denotes that chamber A exhausts and chamber B fills.

Mode 3: u=0 denotes that chambers A and B are both closed.

As the system model uncertainties are unmatched, a recursive backstepping design procedure was adopted to synthesize a DARC law.

3.2.1 Step 1

Define a switching-function-like quantity as

$$e_2=\dot{e}_1+k_1e_1=x_2-x_{2\mathrm{eq}},\ \ x_{2\mathrm{eq}}\triangleq\dot{x}_{1\mathrm{r}}-k_1e_1, \tag{13}$$

where e_1=x_1−$x_{1\mathrm{r}}$ is the output trajectory tracking error, k_1 is any positive feedback gain, and $x_{1\mathrm{r}}$ is the reference trajectory to be tracked by x_1. Making e_2 small or converge to zero is equivalent to making e_1 small or converge to zero, since the transfer function $G(s)$= $1/(s+k_1)$ from e_2 to e_1 is stable. Hence, the objective of this design is to make e_2 as small as possible with a guaranteed transient performance.

Differentiating Eq. (13) and combining with the second equation of Eq. (8), the result appears as

$$\begin{aligned}\theta_1\dot{e}_2=&A_{\mathrm{a}}x_3-A_{\mathrm{b}}x_4-p_0A_{\mathrm{r}}+\theta_2-\theta_3x_2-\theta_4S_{\mathrm{f}}(x_2)\\ &-\theta_1\dot{x}_{2\mathrm{eq}}+\tilde{F}_0.\end{aligned} \tag{14}$$

Define a positive semi-definite function

$$V_2=\frac{1}{2}\theta_1r_2e_2^2, \tag{15}$$

where r_2 is a positive weighting factor. Differentiating Eq. (15) and combining with Eq. (14) lead to

$$\dot{V}_2 = r_2 e_2 (A_a x_3 - A_b x_4 - p_0 A_r + \theta_2 - \theta_3 x_2 - \theta_4 S_f(x_2) - \theta_1 \dot{x}_{2eq} + \tilde{F}_0). \quad (16)$$

Define the output pressure force as $F_p = A_a x_3 - A_b x_4 - p_0 A_r$. Construct the desired output pressure force F_{pd} for the virtual control input F_p and give the adaptation function $\boldsymbol{\tau}_2$ in the form as given in Eq. (17), such that the tracking error converges to zero or a small value with a guaranteed transient performance.

The desired output pressure force F_{pd} and the adaptation function $\boldsymbol{\tau}_2$ are given by

$$\begin{cases} F_{pd} = F_{pda} + F_{pds}, \\ F_{pds} = F_{pds1} + F_{pds2}, \\ F_{pda} = -\hat{\theta}_2 + \hat{\theta}_3 x_2 + \hat{\theta}_4 S_f(x_2) + \hat{\theta}_1 \dot{x}_{2eq}, \\ F_{pds1} = -k_2 e_2, \ k_2 > 0, \\ \boldsymbol{\tau}_2 = r_2 \boldsymbol{\varphi}_2 e_2, \end{cases} \quad (17)$$

where function F_{pda} is an adaptive control part used to achieve improved model compensation through online parameter adaptation. Function F_{pds}, as a robust control law, is composed of two parts, F_{pds1}, stabilizing the nominal system term, and F_{pds2}, the nonlinear robust feedback term synthesized later. $\boldsymbol{\varphi}_2$ is a vector given by $\boldsymbol{\varphi}_2 = [-\dot{x}_{2eq}, 1, -x_2, -S_f(x_2), 0, 0]^T$.

Denote the virtual control input discrepancy as $e_3 = F_p - F_{pd}$. Substituting Eq. (17) into Eq. (16), then

$$\dot{V}_2 = r_2 e_2 e_3 - r_2 k_2 e_2^2 + r_2 e_2 (F_{pds2} - \boldsymbol{\varphi}_2^T \tilde{\boldsymbol{\theta}} + \tilde{F}_0), \quad (18)$$

where the nonlinear robust feedback term F_{pds2} is used to attenuate the effects of the last two terms inside the brackets of Eq. (18) for a guaranteed robust performance (Meng *et al.*, 2013b), which must be chosen to satisfy the following constraint conditions:

$$\begin{cases} e_2 (F_{pds2} - \boldsymbol{\varphi}_2^T \tilde{\boldsymbol{\theta}} + \tilde{F}_0) \le \varepsilon_2, \\ e_2 F_{pds2} \le 0, \end{cases} \quad (19)$$

where ε_2 is the boundary layer thickness, which can be an arbitrarily small positive value. The second condition of Eq. (19) is to ensure the natural dissipation of F_{pds2} without affecting the functionality of the adaptive control part F_{pda}.

To meet the above constraint conditions, F_{pds2} can be chosen as

$$F_{pds2} = -h_2^2(t) e_2 / (4\varepsilon_2), \quad (20)$$

where $h_2(t)$ can be any known bounding function satisfying

$$h_2(t) \ge \left\| \boldsymbol{\varphi}_2^T \right\| \left\| \boldsymbol{\theta}_{max} - \boldsymbol{\theta}_{min} \right\| + F_{max}. \quad (21)$$

Substituting the first inequality of Eq. (19) into Eq. (18), we obtain

$$\dot{V}_2 \le r_2 e_2 e_3 - r_2 k_2 e_2^2 + r_2 \varepsilon_2. \quad (22)$$

3.2.2 Step 2

In step 1, as seen from inequality (22), if e_3 is equal to zero and $\dot{V}_2$ converges to zero, then e_2 will exponentially converge to the ball zone $\{e_2(\infty): e_2(\infty) \le \sqrt{\varepsilon_2 / k_2}\}$. The size of e_2 can be made arbitrarily small by adjusting the controller parameter ε_2 and the feedback gain k_2. Certainly, the final tracking errors e_1 and e_2 will both be bounded. Therefore, the goal of step 2 is to synthesize a control function Q_{Ld} such that e_3 may converge to zero or a small value with a guaranteed transient performance.

According to Eqs. (8) and (17), the dynamics of e_3 are

$$\dot{e}_3 = \frac{A_a nR(\dot{m}_{a,in} T_0 - \dot{m}_{a,out} T_a)}{V_a} - \frac{A_b nR(\dot{m}_{b,in} T_0 - \dot{m}_{b,out} T_b)}{V_b} - \frac{nA_a^2 x_2 x_3}{V_a} - \frac{nA_b^2 x_2 x_4}{V_b} + A_a \theta_5 - A_b \theta_6 + A_a \tilde{D}_{a0} - A_b \tilde{D}_{b0} - \dot{F}_{pd}. \quad (23)$$

In the original DARC (Yao and Tomizuka, 1997), the derivative of the intermediate control law consists of two parts: the calculable part and the incalculable part. The calculable part can be used in the control function design, while the incalculable part, on account of various uncertainties, needs to be dealt with by robust feedback later. In this case, the derivative of the desired output pressure force $\dot{F}_{pd}$ can be

subdivided into two parts: the incalculable part $\dot{F}_{\mathrm{pdu}}=-\dfrac{\partial F_{\mathrm{pd}}}{\partial x_2}\dot{\tilde{x}}_2$ and the calculable part $\dot{F}_{\mathrm{pdc}}=\dfrac{\partial F_{\mathrm{pd}}}{\partial x_1}x_2+\dfrac{\partial F_{\mathrm{pd}}}{\partial x_2}\dot{\hat{x}}_2+\dfrac{\partial F_{\mathrm{pd}}}{\partial t}+\dfrac{\partial F_{\mathrm{pd}}}{\partial \hat{\boldsymbol{\theta}}}\dot{\hat{\boldsymbol{\theta}}}$. As seen from the equation of the calculable part, the solution procedure of the calculable part $\dot{F}_{\mathrm{pdc}}$ needs quite a bit of computation time. Moreover, the more parameters that are estimated, the more computation time may be consumed. The Kalman filter is an optimal recursive estimation algorithm equipped with high computational efficiency. To optimize the control algorithm, a Kalman filter is introduced to predict $\dot{F}_{\mathrm{pd}}$ without affecting the effectiveness of the DARC strategy. The detailed solution is presented in the following.

Choose a positive semi-definite function

$$V_3=\frac{1}{2}\theta_1 r_2 e_2^2+\frac{1}{2}r_3 e_3^2, \tag{24}$$

where r_3 is a positive weighting factor. Differentiating Eq. (24) and combining with Eqs. (18) and (23) yield

$$\dot{V}_3=\dot{V}_2+r_3e_3\big[Q_{\mathrm{L}}-nA_{\mathrm{a}}^2x_2x_3/V_{\mathrm{a}}-nA_{\mathrm{b}}^2x_2x_4/V_{\mathrm{b}}+A_{\mathrm{a}}\theta_5-A_{\mathrm{b}}\theta_6+A_{\mathrm{a}}\tilde{D}_{\mathrm{a}0}-A_{\mathrm{b}}\tilde{D}_{\mathrm{b}0}-\dot{F}_{\mathrm{pd}}\big], \tag{25}$$

where the new virtual control input is

$$Q_{\mathrm{L}}=\frac{A_{\mathrm{a}}nR(\dot{m}_{\mathrm{a,in}}T_0-\dot{m}_{\mathrm{a,out}}T_{\mathrm{a}})}{V_{\mathrm{a}}}-\frac{A_{\mathrm{b}}nR(\dot{m}_{\mathrm{b,in}}T_0-\dot{m}_{\mathrm{b,out}}T_{\mathrm{b}})}{V_{\mathrm{b}}}.$$

Based on a similar consideration of Eq. (17), the desired air mass flow rate Q_{Ld} for the new virtual control input Q_{L} is constructed in the following form:

$$\begin{cases}Q_{\mathrm{Ld}}=Q_{\mathrm{Lda}}+Q_{\mathrm{Lds}},\ Q_{\mathrm{Lds}}=Q_{\mathrm{Lds1}}+Q_{\mathrm{Lds2}},\\ Q_{\mathrm{Lda}}=-e_2r_2/r_3+nA_{\mathrm{a}}^2x_2x_3/V_{\mathrm{a}}+nA_{\mathrm{b}}^2x_2x_4/V_{\mathrm{b}}\\ \qquad -A_{\mathrm{a}}\hat{\theta}_5+A_{\mathrm{b}}\hat{\theta}_6+\dot{F}_{\mathrm{pd}},\\ Q_{\mathrm{Lds1}}=-k_3e_3,\\ \boldsymbol{\tau}=\boldsymbol{\tau}_2+r_3\boldsymbol{\varphi}_3e_3,\end{cases} \tag{26}$$

where k_3 is the feedback gain, which is a constant. Q_{Lda} is used for adjustable model compensation with the parameter estimates $\hat{\boldsymbol{\theta}}_5$ and $\hat{\boldsymbol{\theta}}_6$ updated via the rate-limited projection type adaptation law. Q_{Lds1} is the proportional feedback of e_3 for stabilizing the nominal system, Q_{Lds2} is used to dominate the model uncertainties, and $\boldsymbol{\varphi}_3$ is a vector given by $\boldsymbol{\varphi}_3=[0, 0, 0, 0, A_{\mathrm{a}}, -A_{\mathrm{b}}]^{\mathrm{T}}$.

Suppose that the discrepancy between Q_{L} and Q_{Ld} is non-existent, as the inaccuracy of the mass flow rate model described above is lumped into the modeling error. Then, substituting Eq. (26) into Eq. (25) yields

$$\dot{V}_3=\dot{V}_2-r_2e_2e_3-r_3k_3e_3^2+r_3e_3(Q_{\mathrm{Lds2}}-\boldsymbol{\varphi}_3^{\mathrm{T}}\tilde{\boldsymbol{\theta}}+A_{\mathrm{a}}\tilde{D}_{\mathrm{a}0}-A_{\mathrm{b}}\tilde{D}_{\mathrm{b}0}). \tag{27}$$

Similar to Eq. (19), as a nonlinear robust control function, Q_{Lds2} needs to satisfy the following two constraint conditions for dominating all model uncertainties:

$$\begin{cases}e_3(Q_{\mathrm{Lds2}}-\boldsymbol{\varphi}_3^{\mathrm{T}}\tilde{\boldsymbol{\theta}}+A_{\mathrm{a}}\tilde{D}_{\mathrm{a}0}-A_{\mathrm{b}}\tilde{D}_{\mathrm{b}0})\le\varepsilon_3,\\ e_3Q_{\mathrm{Lds2}}\le 0.\end{cases} \tag{28}$$

Also, to meet the above constraint conditions, Q_{Lds2} can be given by

$$Q_{\mathrm{Lds2}}=-h_3^2(t)e_3/(4\varepsilon_3), \tag{29}$$

where $h_3(t)\ge\left\|\boldsymbol{\varphi}_3^{\mathrm{T}}\right\|\left\|\boldsymbol{\theta}_{\max}-\boldsymbol{\theta}_{\min}\right\|+A_{\mathrm{a}}D_{\mathrm{a}\max}+A_{\mathrm{b}}D_{\mathrm{b}\max}$.

Substituting the first condition of Eq. (19) and the first condition of Eq. (28) into Eq. (27) gives

$$\dot{V}_3\le-r_2k_2e_2^2-r_3k_3e_3^2+r_2\varepsilon_2+r_3\varepsilon_3\le-KV_3+\varepsilon, \tag{30}$$

where $K=\min\{2k_2/\theta_1,\ 2k_3\}$ and $\varepsilon=r_2\varepsilon_2+r_3\varepsilon_3$. After solving the differential equation (30), we obtain

$$V_3(t)\le\exp(-Kt)V_3(0)+\varepsilon[1-\exp(-Kt)]/K. \tag{31}$$

Thus, the error vector $\boldsymbol{e}=[e_2, e_3]^{\mathrm{T}}$ is bounded above. Therefore, e_2 and e_3 will exponentially converge to some balls whose sizes are dominated by r_2, r_3, ε_2, ε_3. So, output tracking error e_1 will also be ultimately bounded.

3.2.3 Step 3

Since the desired air mass flow rate Q_{Ld} has been calculated, the fully open virtual control input can be expressed as follows:

$$Q_{\mathrm{L,F}}=\begin{cases}\dfrac{A_{\mathrm{a}}nRT_0\dot{m}_{\mathrm{A,in}}}{V_{\mathrm{a}}}+\dfrac{A_{\mathrm{b}}nRT_{\mathrm{b}}\dot{m}_{\mathrm{B,out}}}{V_{\mathrm{b}}}, & Q_{\mathrm{Ld}}>0,\\ \dfrac{A_{\mathrm{a}}nRT_{\mathrm{a}}\dot{m}_{\mathrm{A,out}}}{V_{\mathrm{a}}}+\dfrac{A_{\mathrm{b}}nRT_0\dot{m}_{\mathrm{B,in}}}{V_{\mathrm{b}}}, & Q_{\mathrm{Ld}}<0,\end{cases} \tag{32}$$

where $\dot{m}_{\mathrm{A},\bullet}$ and $\dot{m}_{\mathrm{B},\bullet}$ are the mass flows of the non-rod chamber and rod chamber, respectively, when the relevant on/off solenoid valve opens fully.

Thus, the duty cycle commands of the on/off solenoid valves can be obtained by

$$\begin{cases}u_{(\mathrm{a,in;b,out})}=1,\ u_{(\mathrm{a,out;b,in})}=0, & \text{if } Q_{\mathrm{Ld}}>0,\ Q_{\mathrm{L,F}}=0,\\ u_{(\mathrm{a,in;b,out})}=\mathrm{sat}(Q_{\mathrm{Ld}}/Q_{\mathrm{L}}),\ u_{(\mathrm{a,out;b,in})}=0, & \\ \qquad\qquad \text{if } Q_{\mathrm{Ld}}>0,\ Q_{\mathrm{L,F}}\neq 0,\\ u_{(\mathrm{a,in;b,out})}=0,\ u_{(\mathrm{a,out;b,in})}=0, & \text{if } Q_{\mathrm{Ld}}=0,\\ u_{(\mathrm{a,in;b,out})}=0,\ u_{(\mathrm{a,out;b,in})}=\mathrm{sat}(-Q_{\mathrm{Ld}}/Q_{\mathrm{L}}), & \\ \qquad\qquad \text{if } Q_{\mathrm{Ld}}<0,\ Q_{\mathrm{L,F}}\neq 0,\\ u_{(\mathrm{a,in;b,out})}=0,\ u_{(\mathrm{a,out;b,in})}=-1, & \text{if } Q_{\mathrm{Ld}}<0,\ Q_{\mathrm{L,F}}=0,\end{cases} \tag{33}$$

where $u_{\bullet;\bullet}$ denotes the duty cycle of the specific on/off solenoid valve. For example, $u_{\mathrm{a,in}}$ represents the duty cycle of the on/off solenoid valve responsible for charging the non-rod chamber.

The flow characteristics of on/off solenoid valves with 60-Hz frequency have been determined under different duty cycles (Qian *et al.*, 2014). Thus, the relationship between the PWM signal's duty cycle and control law can be obtained (Fig. 2). In addition, since the four on/off solenoid valves come from the same batch, their flow characteristics are roughly the same (Qian *et al.*, 2014).

Remark 1 Since the original system has a dimensionality of four, there are 1D internal dynamics. This means that there are infinite possibilities for p_{a} and p_{b} to synthesize a desired output pressure force $F_{\mathrm{p}}=A_{\mathrm{a}}p_{\mathrm{a}}-A_{\mathrm{b}}p_{\mathrm{b}}-A_{\mathrm{r}}p_0$. At present, a rigorous proof of the internal dynamics has not been given. However, experimental results (pressures in both chambers are bounded) suggest that the internal dynamics are stable.

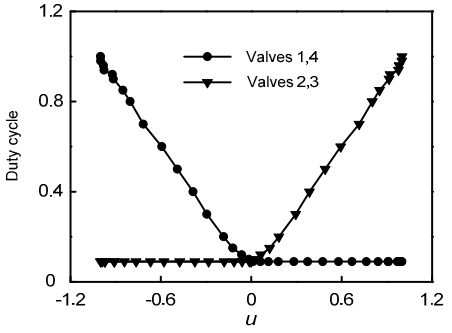

Fig. 2 The relationship between the duty cycle and the control law

4 Kalman filter design

In a motion trajectory tracking system, velocity feedback and acceleration feedback can be introduced into the control loop to improve control performance. Usually, velocity and acceleration are indirectly obtained through the displacement signal from a displacement sensor. Nevertheless, since the measured displacement signal is noisy, directly differentiating this signal causes severe noise amplification. Thus, the objective signal is submerged in the noise. Therefore, direct use of the differential method is inappropriate here.

Conventional digital low-pass filters can be used to obtain relatively smooth velocity and acceleration signals. However, some time delay will inevitably be introduced, possibly bringing instability for a real-time control system. So, a conventional digital low-pass filter is not appropriate.

High performance motion control systems are strict, with real-time capability. An alternative and high computationally efficient solution is to apply a Kalman filter algorithm, which is an optimal recursive estimation algorithm. The Kalman filter is essentially a set of mathematical equations implementing a predictor-corrector type estimator which is optimal in the sense that it minimizes the estimated error covariance when some presumed conditions are met (Welch and Bishop, 2001). Usually, it is employed for online filtering, especially in real-time tracking control systems.

Due to the low mobility of the tracked target signal, the model assumes constant acceleration between sampling times. The canonical discrete state description of the system model can be stated as

$$\begin{cases}\boldsymbol{X}[k+1]=\boldsymbol{A}_d\boldsymbol{X}[k]+\boldsymbol{W}_d w[k],\\ z[k]=\boldsymbol{H}_d\boldsymbol{X}[k]+v[k],\end{cases} \tag{34}$$

where z is the measurement. For motion states,

$$\boldsymbol{X}[k]=\begin{bmatrix}x[k]\\ v[k]\\ a[k]\end{bmatrix},\ \boldsymbol{A}_d=\begin{bmatrix}1 & T_\mathrm{s} & T_\mathrm{s}^2/2\\ 0 & 1 & T_\mathrm{s}\\ 0 & 0 & 1\end{bmatrix},\ \boldsymbol{W}_d=\begin{bmatrix}T_\mathrm{s}^2/2\\ T_\mathrm{s}\\ 1\end{bmatrix},$$

$$\boldsymbol{H}_d=[1\ 0\ 0];$$

with respect to the derivative of the intermediate control law (the desired output pressure force),

$$\boldsymbol{X}[k]=\begin{bmatrix}F_\mathrm{pd}[k]\\ \dot{F}_\mathrm{pd}[k]\end{bmatrix},\ \boldsymbol{A}_d=\begin{bmatrix}1 & T_\mathrm{s}\\ 0 & 1\end{bmatrix},\ \boldsymbol{W}_d=\begin{bmatrix}T_\mathrm{s}^2/2\\ T_\mathrm{s}\end{bmatrix},\ \boldsymbol{H}_d=[1\ 0].$$

The random variables w and v represent the process and measurement noises, respectively. Both are white noises whose covariances Q and R can be chosen empirically.

The Kalman filter estimates a process using a form of feedback control; i.e., the filter estimates the process state at some time and then obtains feedback in the form of (noisy) measurements. As such, the complete set of the corresponding discrete Kalman filter formulation consists of time update equations and measurement update equations. The time update equations are responsible for projecting forward (in time) the current state and error covariance estimates to obtain the a priori estimates for the next time step. The measurement update equations are responsible for the feedback, i.e., for incorporating a new measurement into the a priori estimate to obtain an improved a posteriori estimate (Welch and Bishop, 2001). The time update equations are also called prediction equations, shown as

$$\begin{cases}\hat{\boldsymbol{x}}(k\mid k-1)=\boldsymbol{A}_d\hat{\boldsymbol{x}}(k-1),\\ \boldsymbol{P}(k\mid k-1)=\boldsymbol{A}_d\boldsymbol{P}(k-1)\boldsymbol{A}_d^\mathrm{T}+\boldsymbol{W}_d\boldsymbol{Q}\boldsymbol{W}_d^\mathrm{T},\end{cases} \tag{35}$$

where $\boldsymbol{P}$ represents the error covariance matrices. The measurement update equations, also known as the corrector equations, are given by

$$\begin{cases}\boldsymbol{K}(k)=\boldsymbol{P}(k\mid k-1)\boldsymbol{H}_d^\mathrm{T}[\boldsymbol{H}_d\boldsymbol{P}(k\mid k-1)\boldsymbol{H}_d^\mathrm{T}+R_d]^{-1},\\ \hat{\boldsymbol{x}}(k)=\hat{\boldsymbol{x}}(k\mid k-1)+\boldsymbol{K}(k)[z(k)-\boldsymbol{H}_d\boldsymbol{A}_d\hat{\boldsymbol{x}}(k-1)],\\ \boldsymbol{P}(k)=[\boldsymbol{I}-\boldsymbol{K}(k)\boldsymbol{H}_d]\boldsymbol{P}(k\mid k-1)[\boldsymbol{I}-\boldsymbol{K}(k)\boldsymbol{H}_d]^\mathrm{T}\\ \qquad\quad +\boldsymbol{K}(k)R_d\boldsymbol{K}^\mathrm{T}(k),\end{cases} \tag{36}$$

where $\boldsymbol{K}$ denotes the Kalman gain matrices, R_d=R.

5 Implementation and results

5.1 Experimental apparatus

To evaluate the performance of the proposed modified DARC, an experimental apparatus was set up. A schematic diagram of the solenoid valve-controlled pneumatic cylinder system is given in Fig. 3. The actuator pneumatic cylinder (FESTO AND-100-50-A-P-A-S11) was controlled by on/off valves (FESTO MHE3-MS1H-3/2G-1/8-K, configured as a two-way valve). Pressures in the tank and both chambers were measured by three pressure sensors (Huba 511.930003741). The position data of the piston movement were obtained by a resistance type linear position sensor (NOVOTECHNIK LWH75). Velocity and acceleration were both estimated by the Kalman filter as described in the previous section. The data acquire card (NI PCI-6251) acquired all the signals of the above-mentioned sensors. A circuit board with a four-channel PWM drive circuit was developed for the synchronous updates of four duty cycles. Here, the frequency of PWM waves was set to 60 Hz. The control algorithm was realized by computer and the sampling period was 4 ms. The main model parameters of the system were: A_a=7.854×10^{-3} m^2, A_b=7.54×10^{-3} m^2, b_v=3500 N·s/m, $V_{0\mathrm{a}}$=5.036×10^{-5} m^3, $V_{0\mathrm{b}}$=2.916×10^{-5} m^3, C=8.373×10^{-9} m^3/(s·Pa), b=0.18561, L=0.05 m, n=1.2, R=287 N·m/(kg·K), T_s=283.15 K, p_s=6×10^5 Pa, and p_0=1.01325×10^5 Pa. The nominal values of the system model's uncertain parameters were set as θ_1=0.9389 kg, θ_2=0 N, θ_3=3500 N·s/m, θ_4=100 N, θ_5=0 Pa/s, θ_6=0 Pa/s. The bounds of the uncertain parameters were selected as $\boldsymbol{\theta}_\mathrm{min}$=[0.5, −10, 2000, −50, −20, −20]$^\mathrm{T}$ and $\boldsymbol{\theta}_\mathrm{max}$=[5, 10, 5000, 200, 20, 20]$^\mathrm{T}$. For online updating of the uncertain parameters, the diagonal adaptation rate matrix was chosen as $\boldsymbol{\Gamma}$=diag(0.2, 300, 2000, 500, 100, 100) and the preset adaptation rate limit was set as $\dot{\boldsymbol{\theta}}_M$=[50, 500, 2000, 100, 50, 50]$^\mathrm{T}$.

The proposed modified controller parameters for the experimental implementation after trial-and-error were k_1=65, k_2=6700, k_3=50, h_2=10, h_3=100, ε_2=0.05, ε_3=250. The weighting factors r_2 and r_3 were set as 1 and 0.1, respectively. In addition, the covariances Q and R of the random variables w and v, respectively, in the above Kalman filter were Q=3100 and R=0.0001.

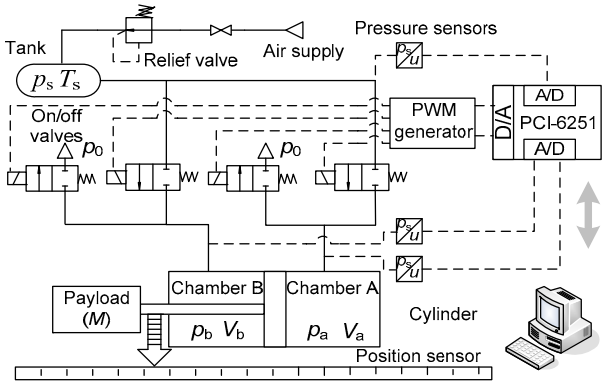

Fig. 3 Schematic diagram of the experimental apparatus

To evaluate the trajectory tracking performance, the following two performance indices were used:

1. E_p=max$_{\text{last }3T}\{e_1\}$, the absolute value of the peak tracking error during the last three periods, was used as an index evaluating the final tracking performance.

2. $E_{\text{rms}}=\sqrt{\dfrac{1}{3T}\int_{T_e-3T}^{T_e}e_1^2\mathrm{d}t}$, the root-mean-square value of the tracking error during the last three periods, was used as an index evaluating the average tracking performance, where T and T_e represent the reference trajectory signal period and the entire tracking time, respectively.

5.2 Sinusoidal trajectory tracking

To verify the tracking performance of the proposed controller in the solenoid valve-controlled pneumatic cylinder system, a set of experiments tracking sinusoidal trajectories was first conducted. Figs. 4 and 5 show experimental results from adopting the proposed modified DARC for tracking sinusoidal trajectories with an amplitude of 17.5 mm and frequencies of 0.5 and 0.75 Hz, respectively. Table 1 shows the detailed results of tracking reference trajectories with the modified DARC in terms of performance indices. The final tracking peak error was about 0.43 mm or 2.4% of the input signal amplitude, and the average tracking error was 0.19 mm (Fig. 4). These values are relatively small compared with those in most other studies, especially for a system controlled with solenoid on/off valves. However, due to the existence of friction and low stiffness in the initial stage, there are some considerable errors at the beginning. During the whole operating process, the control pressures of both chambers were bounded (Fig. 6), which suggests the internal dynamics were stable. Fig. 7 shows the online parameter estimates of the entire 0.5 Hz sinusoidal trajectory tracking process with the modified DARC. Apparently, the estimates of parameters were all convergent and can stay around some constant values. Since the reference trajectory does not always satisfy the persistent exciting (PE) condition, the parameter estimates may converge slowly when the reference trajectory velocity is close to zero. The control input of the proposed modified DARC for tracking the 0.75 Hz sinusoidal trajectory is presented in Fig. 8. Compared with the

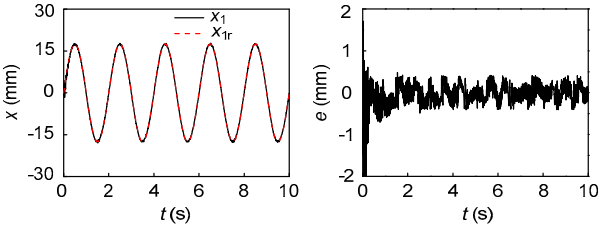

Fig. 4 Tracking results of the modified DARC for a 0.5 Hz sinusoidal trajectory

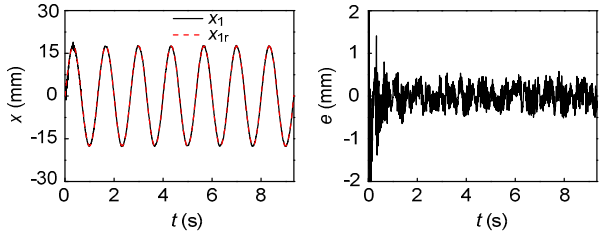

Fig. 5 Tracking results of the modified DARC for a 0.75 Hz sinusoidal trajectory

Table 1 Experimental results for the modified DARC in terms of performance indices

M (kg)	Trajectory (mm)	E_p (mm)	E_{rms} (mm)
1.05	17.5sin(πt)	0.42	0.19
1.05	17.5sin(1.5πt)	0.53	0.23
2.18	17.5sin(πt)	0.45	0.20
1.05	Smooth square	0.38	0.16

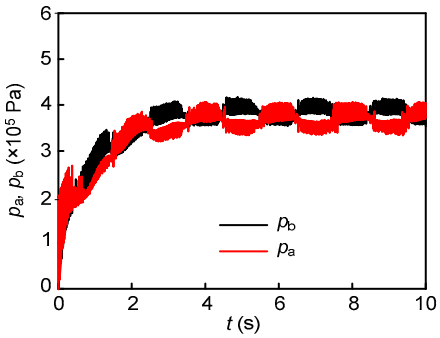

Fig. 6 Chamber pressures for tracking a 0.5 Hz sinusoidal trajectory with the modified DARC

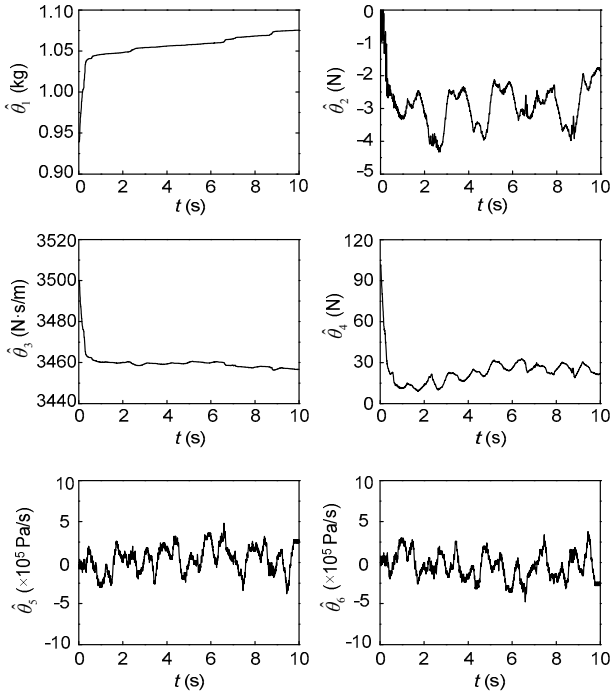

Fig. 7 Parameter estimation for a 0.5 Hz sinusoidal trajectory with the modified DARC

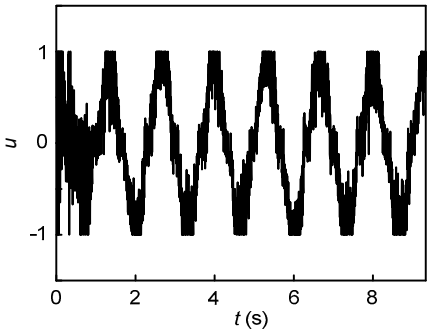

Fig. 8 Control input for a 0.75 Hz sinusoidal trajectory with the modified DARC

results of Carneiro and de Almeida (2012), the control signal input chattering was within the acceptable range, especially as we were using solenoid on/off valves.

For comparison with the modified DARC, the original DARC without any retuning of the parameters was employed to track the same reference trajectory as in Fig. 5. The experimental results were presented in Figs. 9 and 10, and the tracking errors in terms of performance indices were 0.52 and 0.23 mm, respectively. Whether considering the final tracking performance or the average tracking performance, the modified DARC was no less favorable compared with the original DARC. The boundedness of both chamber pressures (Fig. 10) once again suggests that the internal dynamics were stable.

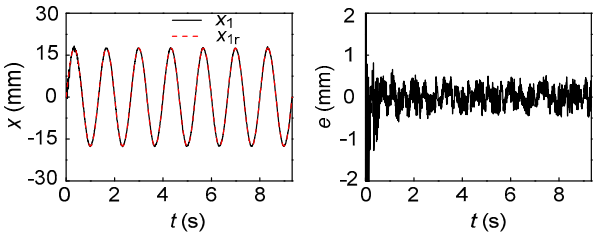

Fig. 9 Tracking results of DARC for a 0.75 Hz sinusoidal trajectory

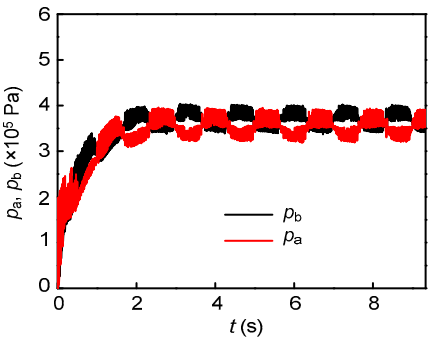

Fig. 10 Chamber pressures for tracking a 0.75 Hz sinusoidal trajectory with the DARC

In addition, a set of experiments was performed in which the derivative of the intermediate control law $\dot{F}_{\mathrm{od}}$ was obtained from direct differentiation of the desired output pressure force. Fig. 11 shows the corresponding experimental results for tracking the same reference trajectory as in Fig. 4. Clearly, since directly differentiating the intermediate control law resulted in quite noisy data under the same conditions, the

system appeared to be subject to quite severe chattering. In comparison with Fig. 11, Fig. 4 illustrates that the proposed modified DARC is effective.

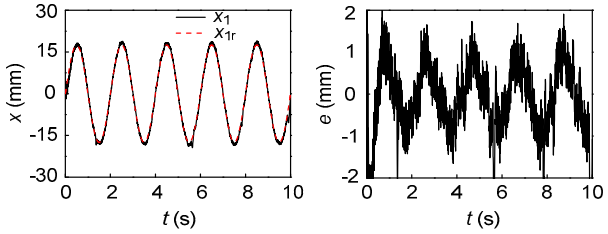

Fig. 11 Tracking results of the DARC (direct differentiation of the intermediate control law) for a 0.5 Hz sinusoidal trajectory

5.3 Smooth square tracking

To test the proposed controller's positioning performance, an experiment involving tracking a smooth square instead of a square wave (Fig. 12) was performed. Since the reference trajectory was not persistently exciting, a constraint that the parameters were updated only when the velocity of the desired trajectory was over 0.001 m/s was set. The final tracking error was E_p=0.38 mm, and the average tracking error E_{rms}=0.16 mm (Fig. 13). The process of parameter estimation is shown in Fig. 14.

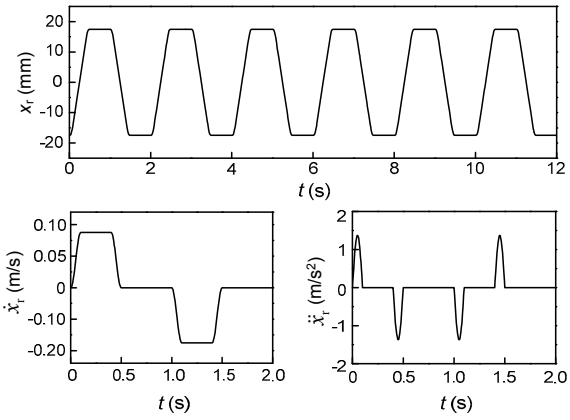

Fig. 12 Smooth square trajectory

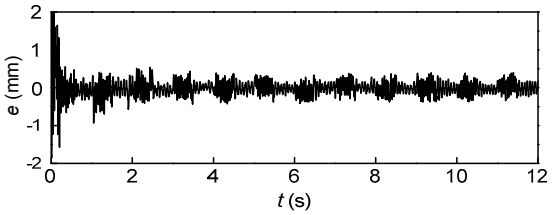

Fig. 13 Tracking error of the modified DARC for a 0.5 Hz smooth square trajectory

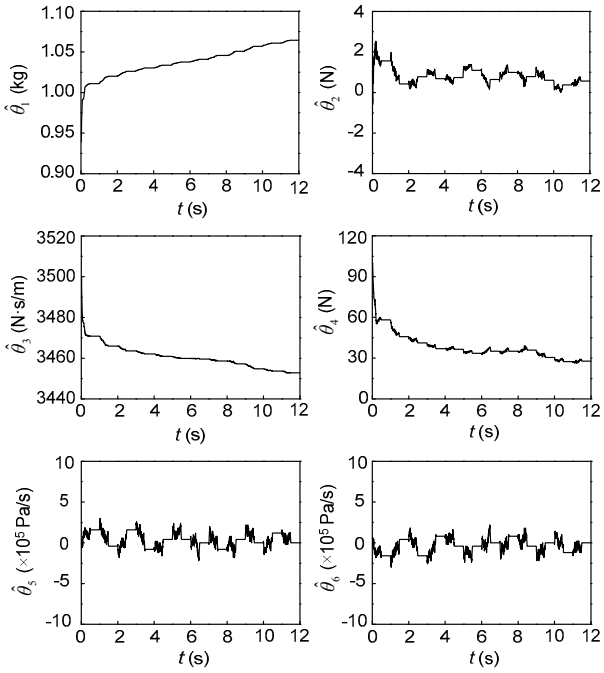

Fig. 14 Parameter estimation for a 0.5 Hz smooth square trajectory with the modified DARC

5.4 Robustness tests

To test the robustness of the proposed controller when faced with payload changes or a sudden disturbance, related experiments were conducted without any controller retuning. The tracking error of a 0.5 Hz sinusoidal trajectory with an additional 1.136 kg load is shown in Fig. 15 and the experimental results in terms of performance indices are shown in Table 1. Owing to the use of online parameter adaptation (Fig. 16), the proposed controller can cope well with payload changes. Fig. 17 shows the experimental results of tracking a 0.5 Hz sinusoidal trajectory with a sudden disturbance. A sudden disturbing force (about 30 N) was added to the moving parts at t=7.6 s, enhanced (up to 80 N) at t=9.8 s, and completely removed at t=11.9 s. Apparently, the

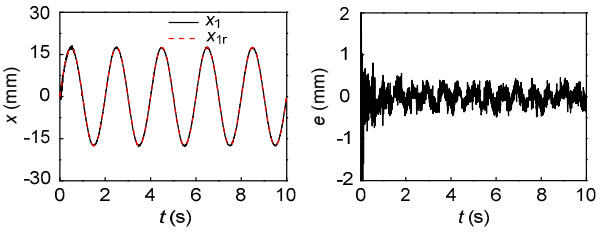

Fig. 15 Tracking results of the modified DARC for a 0.5 Hz sinusoidal trajectory with an additional 1.136 kg load

sudden disturbance had no effect on the tracking performance, except for the transient spikes when the disturbing force changed abruptly. This shows that the proposed controller is robust to sudden disturbances.

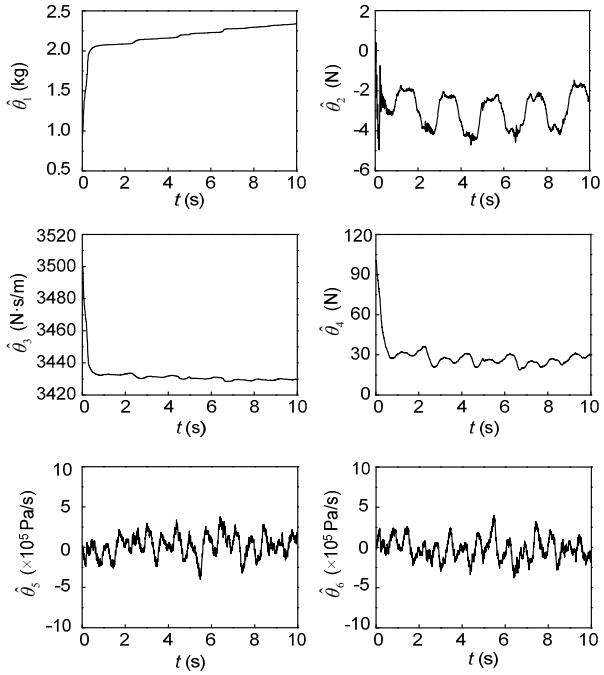

Fig. 16 Parameter estimation of the modified DARC for a 0.5 Hz sinusoidal trajectory with an additional 1.136 kg load

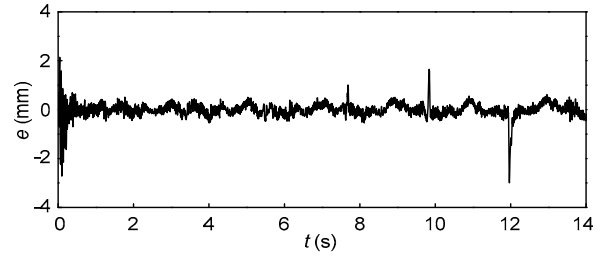

Fig. 17 Tracking error of the modified DARC for a 0.5 Hz sinusoidal trajectory with a disturbance

6 Conclusions

A modified DARC controller was developed for achieving high-precision motion trajectory tracking control of a pneumatic cylinder driven by four costless on/off solenoid valves with PWM. The controller presented consists of two main parts: a gradient type online adaptation for obtaining accurate estimates of unknown model parameters, and a robust control law for weakening the effects of unmodeled dynamics, disturbances, and parameter estimation errors. Kalman filters are employed to predict not only the derivative of the intermediate control law, but also velocity and acceleration. Thus, the process of solving the calculable part from the derivative of the intermediate control law in the original DARC strategy can be removed and the control algorithm can be simplified. Because of unmatched model uncertainties, recursive backstepping technology is applied. By using discontinuous projection mapping, the parameter adaptation law and the robust control law can be synthesized simultaneously. Experimental results illustrate the effectiveness of the proposed controller.

References

Ahn, K., Yokota, S., 2005. Intelligent switching control of pneumatic actuator using on/off solenoid valves. *Mechatronics*, **15**(6):683-702. [doi:10.1016/j.mechatronics.2005.01.001]

Aziz, S., Bone, G.M., 1998. Automatic tuning of an accurate position controller for pneumatic actuators. Proc. IEEE/RSJ Int. Conf. on Intelligent Robots and Systems, p.1782-1788. [doi:10.1109/IROS.1998.724855]

Barth, E.J., Goldfarb, M., 2002. A control design method for switching systems with application to pneumatic servo systems. ASME Int. Mechanical Engineering Congress and Exposition, p.463-469. [doi:10.1115/IMECE2002-33424]

Barth, E.J., Zhang, J., Goldfarb, M., 2002. Sliding mode approach to PWM-controlled pneumatic systems. Proc. American Control Conf., **3**:2362-2367. [doi:10.1109/ACC.2002.1023995]

Brun, X., Belgharbi, M., Sesmat, S., *et al.*, 1999. Control of an electropneumatic actuator: comparison between some linear and non-linear control laws. *Proc. Inst. Mech. Eng. Part I: J. Syst. Contr. Eng.*, **213**(5):387-406. [doi:10.1243/0959651991540232]

Carneiro, J.F., de Almeida, F.G., 2012. A high-accuracy trajectory following controller for pneumatic devices. *Int. J. Adv. Manuf. Technol.*, **61**(1-4):253-267. [doi:10.1007/s00170-011-3695-6]

Chen, H.M., Chen, Z.Y., Chung, M.C., 2009. Implementation of an integral sliding mode controller for a pneumatic cylinder position servo control system. 4th Int. Conf. on Innovative Computing, Information and Control, p.552-555. [doi:10.1109/ICICIC.2009.240]

Girin, A., Plestan, F., Brun, X., *et al.*, 2009. High-order sliding-mode controllers of an electropneumatic actuator: application to an aeronautic benchmark. *IEEE Trans. Contr. Syst. Technol.*, **17**(3):633-645. [doi:10.1109/TCST.2008.2002950]

Hodgson, S., Le, M.Q., Tavakoli, M., *et al.*, 2012. Improved tracking and switching performance of an electropneumatic positioning system. *Mechatronics*, **22**(1):1-12.

[doi:10.1016/j.mechatronics.2011.10.007]

Lee, H.K., Choi, G.S., Choi, G.H., 2002. A study on tracking position control pneumatic actuators. *Mechatronics*, **12**(6):813-831. [doi:10.1016/S0957-4158(01)00024-1]

Meng, D.Y., Tao, G.L., Ban, W., *et al.*, 2013a. Adaptive robust output force tracking control of pneumatic cylinder while maximizing/minimizing its stiffness. *J. Cent. South Univ.*, **20**(6):1510-1518. [doi:10.1007/s11771-013-1642-4]

Meng, D.Y., Tao, G.L., Zhu, X.C., 2013b. Integrated direct/indirect adaptive robust motion trajectory tracking control of pneumatic cylinders. *Int. J. Contr.*, **86**(9):1620-1633. [doi:10.1080/00207179.2013.792002]

Nguyen, T., Leavitt, J., Jabbari, F., 2007. Accurate sliding-mode control of pneumatic systems using low-cost solenoid valves. *IEEE/ASME Trans. Mechatron.*, **12**(2):216-219. [doi:10.1109/TMECH.2007.892821]

Ning, S., Bone, G.M., 2005. Experimental comparison of two pneumatic servo position control algorithms. Proc. IEEE Int. Conf. on Mechatronics and Automation, p.37-42. [doi:10.1109/ICMA.2005.1626519]

Qian, P.F., Tao, G.L., Chen, J.F., 2012. Modeling and simulation of stick-slip motion for pneumatic cylinder based on meter-in circuit. *Appl. Mech. Mater.*, **130-134**:775-780. [doi:10.4028/www.scientific.net/AMM.130-134.775]

Qian, P.F., Tao, G.L., Meng, D.Y., *et al.*, 2014. Nonlinear model-based position servo control of electro-pneumatic clutch actuator. *Trans. Chin. Soc. Agric. Mach.*, **45**(3):1-6 (in Chinese). [doi:10.6041/j.issn.1000-1298.2014.03.001]

Rao, Z., Bone, G.M., 2008. Nonlinear modeling and control of servo pneumatic actuators. *IEEE Trans. Contr. Syst. Technol.*, **16**(3):562-569. [doi:10.1109/TCST.2007.912127]

Richard, E., Scavarda, S., 1996. Comparison between linear and nonlinear control of an electropneumatic servodrive. *J. Dynam. Syst. Meas. Contr.*, **118**(2):245-252. [doi:10.1115/1.2802310]

Richardson, R., Plummer, A.R., Brown, M.D., 2001. Self-tuning control of a low-friction pneumatic actuator under the influence of gravity. *IEEE Trans. Contr. Syst. Technol.*, **9**(2):330-334. [doi:10.1109/87.911384]

Schulte, H., Hahn, H., 2004. Fuzzy state feedback gain scheduling control of servo-pneumatic actuators. *Contr. Eng. Pract.*, **12**(5):639-650. [doi:10.1016/S0967-0661(03)00148-5]

Shen, X., Zhang, J., Barth, E.J., *et al.*, 2006. Nonlinear model-based control of pulse width modulated pneumatic positioning system. *J. Dynam. Syst. Meas. Contr.*, **128**(3):663-669. [doi:10.1115/1.2232689]

Situm, Z., Pavkovic, D., Novakovic, B., 2004. Servo pneumatic position control using fuzzy PID gain scheduling. *J. Dynam. Syst. Meas. Contr.*, **126**(2):376-387. [doi:10.1115/1.1767857]

Smaoui, M., Brun, X., Thomasset, D., 2006. A study on tracking position control of an electropneumatic system using backstepping design. *Contr. Eng. Pract.*, **14**(8):923-933. [doi:10.1016/j.conengprac.2005.05.003]

Tsai, Y.C., Huang, A.C., 2008. Multiple-surface sliding controller design for pneumatic servo systems. *Mechatronics*, **18**(9):506-512. [doi:10.1016/j.mechatronics.2008.03.006]

van Varseveld, R.B., Bone, G.M., 1997. Accurate position control of a pneumatic actuator using on/off solenoid valves. *IEEE/ASME Trans. Mechatron.*, **2**(3):195-204. [doi:10.1109/3516.622972]

Wang, J., Wang, D.J.D., Moore, P.R., *et al.*, 2001. Modelling study, analysis and robust servocontrol of pneumatic cylinder actuator systems. *IEE Proc.-Contr. Theory Appl.*, **148**(1):35-42. [doi:10.1049/ip-cta:20010238]

Welch, G., Bishop, G., 2001. An introduction to the Kalman filter. SIGGRAPH, Course 8.

Xiang, F., Wikander, J., 2004. Block-oriented approximate feedback linearization for control of pneumatic actuator systems. *Contr. Eng. Pract.*, **12**(4):387-399. [doi:10.1016/S0967-0661(03)00104-7]

Xu, L., Yao, B., 2001. Adaptive robust precision motion control of linear motors with negligible electrical dynamics: theory and experiments. *IEEE/ASME Trans. Mechatron.*, **6**(4):444-452. [doi:10.1109/3516.974858]

Yao, B., 2003. Integrated direct/indirect adaptive robust control of SISO nonlinear systems in semi-strict feedback form. Proc. American Control Conf., p.3020-3025. [doi:10.1109/ACC.2003.1243991]

Yao, B., Palmer, A., 2002. Indirect adaptive robust control of SISO nonlinear systems in semi-strict feedback forms. Proc. 15th IFAC World Congress, p.1050. [doi:10.3182/20020721-6-ES-1901.01052]

Yao, B., Tomizuka, M., 1994. Smooth robust adaptive sliding mode control of robot manipulators with guaranteed transient performance. Proc. American Control Conf., p.1176-1180. [doi:10.1109/ACC.1994.751934]

Yao, B., Tomizuka, M., 1997. Adaptive robust control of SISO nonlinear systems in a semi-strict feedback form. *Automatica*, **33**(5):893-900. [doi:10.1016/S0005-1098(96)00222-1]

Yao, B., Bu, F., Reedy, J., *et al.*, 2000. Adaptive robust motion control of single-rod hydraulic actuators: theory and experiments. *IEEE/ASME Trans. Mechatron.*, **5**(1):79-91. [doi:10.1109/3516.828592]

Zhu, X.C., Tao, G.L., Yao, B., *et al.*, 2008. Adaptive robust posture control of a parallel manipulator driven by pneumatic muscles. *Automatica*, **44**(9):2248-2257. [doi:10.1016/j.automatica.2008.01.015]